Journal of Power Sources 180 (2008) 172–175

Contents lists available at ScienceDirect

Journal of Power Sources

journal homepage: www.elsevier.com/locate/jpowsour

Short communication

A Co–Fe alloy as alternative anode for solid oxide fuel cell

Z.G. Lu, J.H. Zhu*, Z.H. Bi, X.C. Lu

Department of Mechanical Engineering, Tennessee Technological University, Box 5014, Cookeville, TN 38501, USA

ARTICLE INFO

Article history:
Received 18 January 2008
Received in revised form 15 February 2008
Accepted 18 February 2008
Available online 4 March 2008

Keywords:
Solid oxide fuel cell
Ordering reaction
Alloy anode
Co–Fe alloy

ABSTRACT

A new type of Ni-free anode material based on $Co_{0.5}Fe_{0.5}$ + SDC ($Sm_{0.2}Ce_{0.8}O_{1.9}$) was identified and evaluated using the $La_{0.8}Sr_{0.2}Ga_{0.83}Mg_{0.17}O_3$ (LSGM) electrolyte-supported cells. The maximum power densities with humidified hydrogen at 800 °C using Au mesh and Pt mesh as anode current collector were 1.07 and 1.20 W cm^{-2}, respectively, which were comparable to that of the cell with the Ni + SDC anode. The cell with the new anode exhibited reasonable performance stability at 800 °C in hydrogen fuel; furthermore, no noticeable change in cell performance with the $Co_{0.5}Fe_{0.5}$ alloy anode was observed upon ordering reaction in the alloy to form the ordered α′ phase at 650 °C.

1. Introduction

Solid oxide fuel cells (SOFCs) have recently attracted tremendous interest because of their high efficiency, low pollutant emission, and flexible fuel choices. Conventional Ni + YSZ (ytttia-stabilized zirconia) cermet anode suffers some serious problems in certain applications, such as detrimental reaction with the (La,Sr)(Ga,Mg)O_3 electrolyte to form electrically insulating layers [1], coking in hydrocarbon fuels [2], sulfur poisoning [3–5], etc. The poor sulfur tolerance of Ni requires that the H_2S contaminant in the fuel must be kept at a very low concentration, e.g. below 1 ppm, to maintain the good performance of the anode, which increases the operation cost of fuel cell and therefore impedes its commercialization. Significant efforts have been made to identify alternative anode materials that will have better catalytic activity and improved sulfur tolerance and can directly operate on hydrocarbon fuels. Two successful examples are the $La_{0.75}Sr_{0.25}Cr_{0.5}Mn_{0.5}O_3$ perovskite and $Sr_2Mg_{1-x}Mn_xMoO_{6-\delta}$ double perovskite, reported by Tao and Irvine and Huang et al., respectively [6,7]. Another approach to improve the anode performance is through alloying addition of other transition metals into Ni to form bimetallic or trimetallic alloys, especially Fe, Cu and Co [8]. Ni–Fe bimetal mixed with YSZ, SDC (samaria-doped ceria) or (La,Sr)(Ga,Mg)O_3 has been demonstrated to possess a noticeably improved performance over the Ni cermet anodes [9–12]. Although the steam reforming activity of CH_4 on Fe–YSZ anode was much lower than on Ni–YSZ at open circuit, the Fe–YSZ anode exhibited excellent coking resistance [13]. The study on the CoNi–YSZ cermets anode for the oxidation of H_2 and CH_4 indicated that the Co content in the CoNi–YSZ anodes had negligible effect on the cell performance with H_2 fuel, while Co addition increased the cell performance with CH_4 [14]. The Ni alloy with 20–25 at.% Fe exhibited an significantly improved performance in H_2 over the pure Ni [12], which is likely related to the presence of the Ni_3Fe phase in the alloy. Trimetal Fe–Co–Ni alloys also were investigated as anode for SOFC based on the GDC ($Ce_{0.9}Gd_{0.1}O_{1.95}$) electrolyte; the $Fe_{0.25}Co_{0.25}Ni_{0.5}$–SDC anode possessed much better electrochemical performance than Ni–SDC [15]. Most alloy anodes studied so far are based on Ni substituted by Co or/and Fe; Ni-free alloys such as the Co–Fe alloy system have not been evaluated as the anode material of SOFCs.

In the present study, we explore the potential of a new type of Ni-free anode based on the $Co_{0.5}Fe_{0.5}$ alloy. The binary Co–Fe alloy system is of interest primarily because both Co and Fe have been used as effective alloying elements for enhancing the performance of the Ni-based anodes. Co has very similar catalytic properties as Ni and less propensity toward carbon deposition, while Fe was also extensively investigated at the early stage of anode development. Furthermore, according to the binary Co–Fe phase diagram [16], the alloy with the composition of $Co_{0.5}Fe_{0.5}$ forms a complete solid solution (α) at the temperature range of 730–985 °C; upon cooling to below 730 °C, an ordering reaction occurs, which leads to the formation of the ordered α′ phase. Such ordering reaction might modify the catalytic activity of the alloy. Therefore, the alloy $Co_{0.5}Fe_{0.5}$ was selected for evaluation as a potential anode material.

2. Experimental

The $La_{0.8}Sr_{0.2}Ga_{0.83}Mg_{0.17}O_3$ (LSGM) electrolyte was used as the support in the single cells. The LSGM powder was synthesized

* Corresponding author. Tel.: +1 931 372 3186; fax: +1 931 372 6340.
E-mail address: jzhu@tntech.edu (J.H. Zhu).

0378-7753/$ – see front matter © 2008 Elsevier B.V. All rights reserved.
doi:10.1016/j.jpowsour.2008.02.051

through a conventional solid-state reaction procedure reported elsewhere [17]. The LSGM powder was pressed into thin pellets with a diameter of 25.4 mm and thickness of 0.9 mm at a pressure of 40 MPa. The pellets were sintered at 1470 °C for 10 h in air, followed by furnace cooling. The sintered pellets were then ground on both sides to a thickness of 0.3 mm as the electrolyte support. X-ray diffraction (XRD) results confirmed that a pure perovskite phase was achieved. The $Co_{0.5}Fe_{0.5}$ oxides, samaria-doped ceria ($Sm_{0.2}Ce_{0.8}O_{1.9}$, SDC) and $SrCo_{0.2}Fe_{0.8}O_{3-\delta}$ (SCF) cathode powders were synthesized through the Pechini method. The as-synthesized powders were calcined at 800 °C for 5 h and ball-milled for 0.5 h. The $Co_{0.5}Fe_{0.5}$ oxide and SDC powders (the weight percentage of the reduced metal was about 50 wt.% in the anode mixture) were thoroughly mixed and ball-milled for 0.5 h prior to screen-printing.

The $Co_{0.5}Fe_{0.5}$ + SDC/SDC/LSGM/SCF cell assembly was prepared with the following procedure. First, an SDC interlayer was deposited on the anode side of the LSGM electrolyte by screen-printing a slurry of the SDC ink. The $Co_{0.5}Fe_{0.5}$ + SDC anode was then screen-printed atop the SDC interlayer. The bi-layer was co-fired at 1300 °C for 0.5 h. The SCF cathode coating was also screen-printed on the opposite side of the LSGM electrolyte and additional cathode paste was added to embed the Pt mesh inside the cathode paste for current collection; the cathode layer with the embedded Pt mesh was fired at 1100 °C for 0.5 h. On the anode side, Au mesh with several separate dots of Au paste was selected for current collection. For comparison, Pt mesh and Pt paste were also used in some cells to replace the Au mesh/paste for the anode-side current collection. The effective working electrode area was 0.24 cm^2. Reference electrodes consisting of the same materials as working electrodes were deposited on the LSGM disc about 2.5 mm away from working electrodes. The reference electrodes were used to monitor the overpotentials of the anode and cathode.

The single cells were sealed onto an Al_2O_3 tube by a Pyrex glass. The assembled test cell was placed in a vertical furnace with the cathode exposed to the ambient air and the anode to humidified hydrogen with a flow rate of 30 ml min^{-1}. A thermocouple was placed near the cell to monitor the testing temperature. The cell performance measurements were carried out at different temperatures using a Solartron 1287 potentiostat with a LabView program. The electrochemical impedance spectrum (EIS) of the single cell was measured using the electrochemical interface with a frequency response analyzer (Solartron 1260) at 800 °C under the open-circuit voltage (OCV). The cross-sectional microstructure of the single cell after testing was examined by scanning electron microscopy (SEM, FEIXL30 environmental scanning electron microscope).

3. Results and discussion

The cross-sectional view near the anode side of the tested cell with the $Co_{0.5}Fe_{0.5}$ + SDC anode is shown in Fig. 1. The SDC buffer layer was quite dense after sintering and had a thickness of about 10 μm, while the thickness of the porous anode layer was about 20 μm. Good adhesion between the anode, the buffer layer, and the LSGM electrolyte assured adequate contact between these layers. Another function of the thin and dense SDC buffer layer is to prevent the interdiffusion between the alloy and electrolyte, which would otherwise increase the contact resistance of the single cell, as reported by Zhang et al. [18].

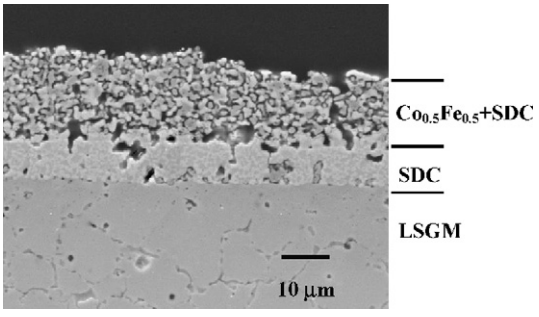

Fig. 1. Cross-sectional view near the $Co_{0.5}Fe_{0.5}$ + SDC anode side of the single cell after cell testing.

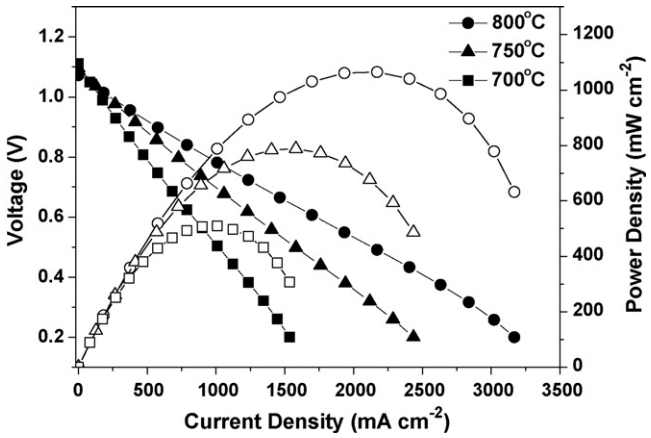

Fig. 2. Voltage (filled symbols) and power density (unfilled symbols) as a function of current density for the Au/$Co_{0.5}Fe_{0.5}$ + SDC/SDC/LSGM/SCF/Pt cell fueled with humidified H_2 at various temperatures.

Fig. 2 gives the voltage and power density as a function of current density for the Au/Co–Fe + SDC/SDC/LSGM/SCF/Pt cell at 700–800 °C. With the Au current collector on the anode side, the maximum power outputs in moist H_2 were 1.07, 0.79 and 0.51 W cm^{-2} at 800, 750 and 700 °C, respectively. The anodic and cathodic overpotentials of the single cell operating at various temperatures are given as a function of current density in Fig. 3. The anodic overpotentials (η_a) were consistently lower than these of the cathode (η_c) at 700–800 °C under the same current density. For example, η_a and η_c at 800 °C at the current density of 2 A cm^{-2} were about 0.2 and 0.3 V, respectively.

To investigate the effect of the ordering reaction in $Co_{0.5}Fe_{0.5}$ on the cell performance, a single cell was first tested at 800 °C, then cooled down and held at 650 °C for several days. The cell performance was monitored as a function of time under a constant current density of 30 mA cm^{-2} at 650 °C in humidified H_2, as shown in Fig. 4. Apparently, the anodic overpotential gradually increased

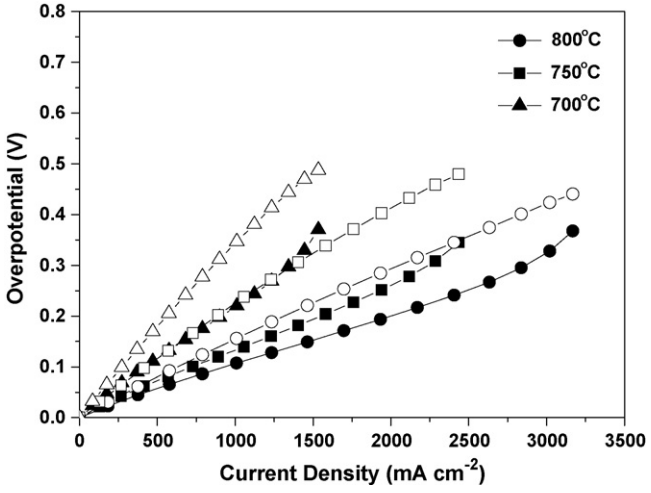

Fig. 3. Overpotentials of anode (filled symbols) and cathode (unfilled symbols) as a function of current density for the single cell operating at various temperatures.

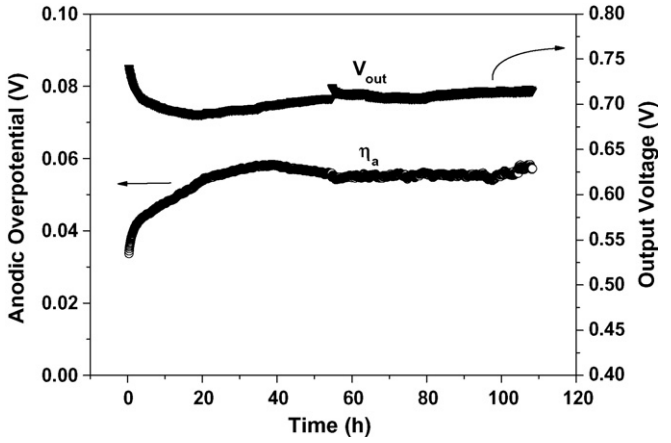

Fig. 4. Variation of the anodic overpotential (η_a) and the cell output voltage (V_{out}) with time at a constant current density of 30 mA cm^{-2} for the single cell at 650 °C in moist H_2.

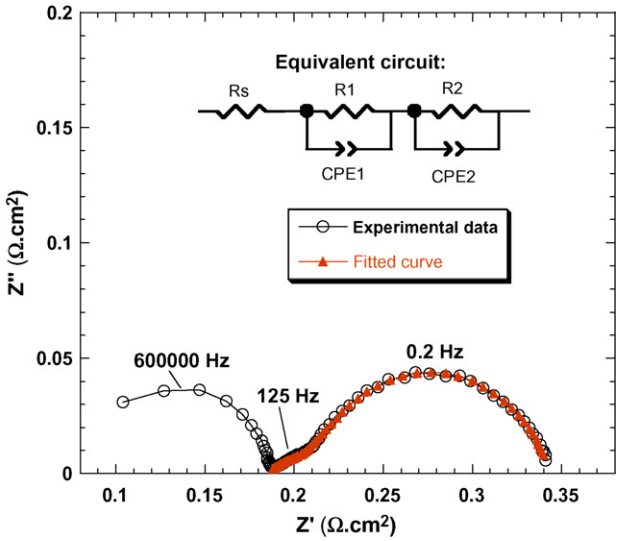

Fig. 6. Impedance spectrum for the $Co_{0.5}Fe_{0.5}$ + SDC/SDC/LSGM/SCF cell at 800 °C in humidified H_2 under OCV. The equivalent circuit for the electrode processes and the corresponding fitted curve were also included.

(while the cell output voltage dropped slightly) during the initial 24-h testing, and no significant change in cell performance was noticed afterwards. This clearly indicates that the ordered α′ phase did not possess enhanced catalytic property for hydrogen decomposition/oxidation over the disordered α phase.

Because the SDC interlayer in this cell structure is also a mixed oxide-ion/electron conductor that is a good catalyst for hydrogen oxidation, it is possible that SDC in the interlayer might contribute to the observed cell performance. To clarify if this is the case, a cell with only the SDC layer as anode and with Au mesh as anode current collector was fabricated and tested under the identical conditions. The maximum power density of the cell with only the SDC layer as anode in moist hydrogen was about 40 mW cm^{-2} at 800 °C, much lower than that of the cell with the $Co_{0.5}Fe_{0.5}$ alloy in the anode. Clearly, the high performance of the cell with the $Co_{0.5}Fe_{0.5}$ alloy anode was not dominated by the SDC layer or SDC in the composite anode; instead, it resulted from the high catalytic activity of the $Co_{0.5}Fe_{0.5}$ alloy for H_2 oxidation.

The performance of the cell with the $Co_{0.5}Fe_{0.5}$ + SDC anode was also measured using the embedded Pt mesh as anode current collector; the cell was fabricated using the same fabrication procedures as reported earlier [12]. The maximum power density of the cell with Pt mesh as anode current collector was about 1.2 W cm^{-2}, as shown in Fig. 5, slightly higher than that of the cell with Au mesh

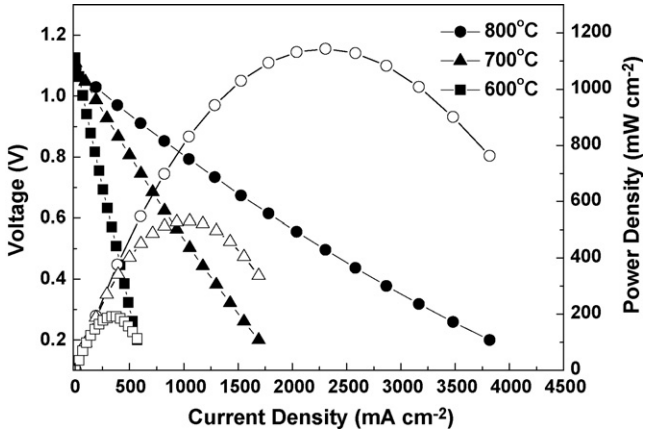

Fig. 5. Voltage (filled symbols) and power density (unfilled symbols) as a function of current density for the Pt/Co–Fe + SDC/SDC/LSGM/SCF/Pt cell fueled with humidified H_2 at various temperatures.

as current collector at 800 °C. Therefore, the type of anode current collectors (Au or Pt) did not significantly affect the cell performance. Compared to the cell performance with the Ni + SDC anode under identical test conditions [12], the $Co_{0.5}Fe_{0.5}$ alloy possessed a similar catalytic activity as the pure Ni.

The impedance spectrum of the single cell with the $Co_{0.5}Fe_{0.5}$ + SDC anode at 800 °C in humidified hydrogen under OCV is shown in Fig. 6. Three depressed semi-circles were detected, with a high-frequency and two low-frequency semi-circles corresponding to the contributions of the electrolyte bulk resistance and the polarization resistance of the electrodes, respectively. The first intercept corresponding to about 0.185 Ω cm^2 is the overall ohmic resistance of the cell (Rs in Fig. 6), which included the ohmic resistance from the electrolyte, the electrodes and the electrolyte–electrode interfaces. Assuming that the ohmic resistance is mainly from the LSGM electrolyte, the calculated ionic conductivity of the electrolyte is about 0.162 S cm^{-1}, very close to the reported value of 0.17 S cm^{-1} for LSGM [19,20]. This indicates that the ohmic resistance from the electrodes and the electrolyte–electrode interfaces was almost negligible compared with that from the electrolyte and the total ohmic resistance of the cell was indeed overwhelmingly dominated by the electrolyte. The low-frequency depressed semi-circles from 4000 to 0.005 Hz corresponding to the electrode processes were fitted using an equivalent circuit shown in Fig. 6, with reasonably good fitting achieved. The arc with a peak frequency of 0.20 Hz had a resistance (R2) of 0.13 Ω cm^2, much higher than R1 for the arc with a peak frequency of 125 Hz (i.e. 0.028 Ω cm^2). The relatively lower polarization resistance of the electrodes compared to the electrolyte resistance implies that further improvement in cell performance might be achieved in the electrode-supported cell configuration.

To evaluate the performance stability of the new alloy anode at high temperature, a single cell with the $Co_{0.5}Fe_{0.5}$ + SDC anode was run in humidified H_2 under a constant current density of 2.0 A cm^{-2} at 800 °C for 40 h. As shown in Fig. 7, during the initial 20 h of testing, there was a slight increase and decrease in anodic and cathodic overpotentials, respectively; subsequently, the overpotentials for both the anode and cathode tended to be stable. The cell output voltage, which is related to the power density of the cell, was almost the same during the 40-h testing. While additional longer-term testing is needed, these initial results indicate that this $Co_{0.5}Fe_{0.5}$ alloy anode promises high and stable performance with H_2 fuel.

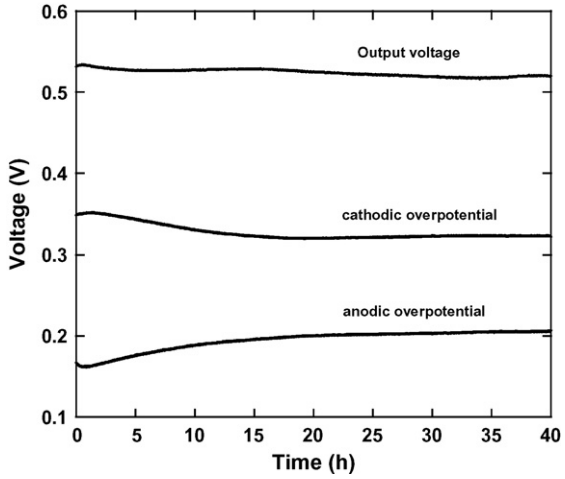

Fig. 7. Cell performance with the $Co_{0.5}Fe_{0.5}$ + SDC anode as a function of time at a constant current density of 2.0 A cm^{-2} at 800 °C in humidified H_2.

4. Conclusions

The $Co_{0.5}Fe_{0.5}$ + SDC cermet was identified as a potential high-performance, Ni-free anode. The cell power density with the new alloy anode reached 1.07–1.20 W cm^{-2} at 800 °C in humidified hydrogen with a 0.3-mm thick LSGM electrolyte, which is comparable to that with the Ni + SDC anode. Ordering reaction in the $Co_{0.5}Fe_{0.5}$ alloy, i.e. formation of an ordered (α') phase at 650 °C, did not noticeably affect the cell performance. The new anode material exhibited adequate performance stability with H_2 fuel.

Acknowledgements

This work was supported by the U.S. Army Communications-Electronics Research, Development and Engineering Center (CERDEC) under contract number W909MY-06-C-0040. Additional support was provided by Tennessee Technological University through a Faculty Research Grant.

References

[1] M. Feng, J.B. Goodenough, K. Huang, C. Milliken, J. Power Sources 63 (1996) 47.
[2] B.C.H. Steele, I. Kelly, H. Middleton, R. Rudkin, Solid State Ionics 28–30 (1988) 1547.
[3] Y. Matsuzaki, I. Yasuda, Solid State Ionics 132 (2000) 261.
[4] D.W. Dees, U. Balachandran, S.E. Dorris, J.J. Heiberger, C.C. McPheeters, J.J. Picciolo, in: S.C. Singhal (Ed.), Proceedings of the First International Symposium on Solid Oxide Fuel Cells, PV 89–91, The Electrochemical Society Proceedings Series, Pennington, NJ (1989), p. 317.
[5] S. Zha, Z. Cheng, M. Liu, J. Electrochem. Soc. 154 (2007) B201.
[6] S. Tao, J.T.S. Irvine, Nat. Mater. 2 (2003) 320.
[7] Y. Huang, R.I. Dass, Z. Xing, J.B. Goodenough, Science 312 (2006) 254.
[8] S. Lee, J.M. Vohs, R.J. Gorte, J. Electrochem. Soc. 151 (2004) A1319.
[9] S. Wang, J. Gao, Electrochem. Solid State Lett. 9 (2006) A395.
[10] A. Ringuedé, D.P. Fagg, J.R. Frade, J. Eur. Ceram. Soc. 24 (2001) 1355.
[11] B. Huang, S.R. Wang, R.Z. Liu, T.L. Wen, J. Power Sources 167 (2007) 288.
[12] X.C. Lu, J.H. Zhu, J. Power Sources 165 (2007) 678.
[13] T. Horita, N. Sakai, T. Kawada, M. Yokokawa, M. Dokiya, J. Electrochem. Soc. 143 (4) (1996) 1161.
[14] K. Sato, Y. Ohmine, K. Ogasa, S. Tsuji, S.C. Singhal, M. Dokiya, SOFC-VIII, vol. 2003-07, Electrochem. Soc., Pennington, NJ, 2003, p. 695.
[15] Z. Xie, W. Zhu, B. Zhu, C. Xia, Electrochim. Acta 51 (2006) 3052.
[16] T.B. Massalski, H. Baker, J.L. Murray, L.H. Bennett, Binary Alloy Phase Diagram, ASM International, 1986.
[17] X.C. Lu, J.H. Zhu, Solid State Ionics 178 (2007) 1467.
[18] X. Zhang, S. Ohara, H. Okawa, R. Maric, T. Fukui, Solid State Ionics 139 (2001) 145.
[19] K. Huang, R.S. Tichy, J.B. Goodenough, J. Am. Ceram. Soc. 81 (1998) 2565.
[20] Z. Bi, Y. Dong, M. Cheng, B. Yi, J. Power Sources 161 (2006) 34.